Redox Biology 26 (2019) 101253

Contents lists available at ScienceDirect

Redox Biology

journal homepage: www.elsevier.com/locate/redox

The fatty acid oxidation enzyme long-chain acyl-CoA dehydrogenase can be a source of mitochondrial hydrogen peroxide

Yuxun Zhang, Sivakama S. Bharathi, Megan E. Beck, Eric S. Goetzman*

Department of Pediatrics, Division of Medical Genetics, University of Pittsburgh School of Medicine, Children's Hospital of Pittsburgh, 4401 Penn Avenue, Pittsburgh, PA, 15224, USA

ARTICLE INFO

Keywords:
Hydrogen peroxide/mitochondria/fatty acid oxidation/acyl-CoA dehydrogenase

ABSTRACT

Fatty acid oxidation (FAO)-driven H_2O_2 has been shown to be a major source of oxidative stress in several tissues and disease states. Here, we established that the mitochondrial flavoprotein long-chain acyl-CoA dehydrogenase (LCAD), which catalyzes a key step in mitochondrial FAO, directly produces H_2O_2 *in vitro* by leaking electrons to oxygen. Kinetic analysis of recombinant human LCAD showed that it produces H_2O_2 15-fold faster than the related mitochondrial enzyme very long-chain acyl-CoA dehydrogenase (VLCAD), but 50-fold slower than a *bona fide* peroxisomal acyl-CoA oxidase. The rate of H_2O_2 formation by human LCAD is slow compared to its activity as a dehydrogenase (about 1%). However, expression of hLCAD in HepG2 cells is sufficient to significantly increase H_2O_2 in the presence of fatty acids. Liver mitochondria from LCAD−/− mice, but not VLCAD−/− mice, produce significantly less H_2O_2 during incubation with fatty acids. Finally, we observe highest LCAD expression in human liver, followed by kidney, lung, and pancreas. Based on our data, we propose that the presence of LCAD drives H_2O_2 formation in response to fatty acids in these tissues.

1. Introduction

Mitochondrial fatty acid β-oxidation (FAO), the process by which fatty acids are chain-shortened for energy generation, has been implicated as a source of H_2O_2 in numerous tissues [1–7]. Identifying the specific sites and sources of FAO-driven H_2O_2 is critical for understanding the role of oxidative stress in the pathogenesis of diseases associated with altered FAO. Recent experiments with isolated liver, kidney, and muscle mitochondria suggest that a substantial portion of FAO-driven H_2O_2 is released in the matrix by flavoproteins upstream of respiratory chain Complex III [3,5,6,8]. These flavoproteins include the short, medium, long, and very long chain acyl-CoA dehydrogenases (ACADs; dubbed SCAD, MCAD, LCAD, and VLCAD), their common redox partner electron transfer flavoprotein (ETF), and electron transfer flavoprotein dehydrogenase (ETFDH). Electrons flow from the ACADs to ETF to ETFDH, an inner mitochondrial membrane protein that passes electrons to ubiquinone and ultimately to Complex III. There are human inborn errors of metabolism associated with mutations in all of these genes except LCAD [9].

Despite the ETF: ETFDH redox couple being the convergence point for a wide variety of acyl-CoA substrates (short, medium, and long-chain fatty acids as well as several branched-chain amino acids), it is generally the long-chain fatty acid substrates that are associated with elevated mitochondrial superoxide and H_2O_2 production [7,10–12]. There are two ACAD enzymes upstream of ETF: ETFDH that utilize long-chain acyl-CoA substrates—LCAD and VLCAD. VLCAD was previously implicated as a source of mitochondrial H_2O_2 and was shown to directly produce H_2O_2 when incubated with long-chain substrates *in vitro* [13]. LCAD, whose role in human FAO has been questioned due to low or absent expression in highly FAO-dependent tissues such as heart and muscle [14,15], has not been evaluated as a possible source of H_2O_2. LCAD is unique among the ACADs for being downregulated in several human cancers, particularly hepatocellular carcinoma (HCC) [16–18]. In the present work, we compared the relative H_2O_2-generating capacity of LCAD and VLCAD. Possible inter-species differences were addressed by comparing H_2O_2 production by both mouse and human recombinant LCAD and VLCAD enzymes. LCAD— particularly human LCAD—was found to generate significantly more H_2O_2 than VLCAD. We further studied LCAD-associated H_2O_2 generation using loss-of-function (LCAD knockout mouse liver mitochondria) and gain-of-function (HepG2 LCAD re-expression) approaches. The presence or absence of LCAD was sufficient to modulate FAO-associated H_2O_2 generation in intact mitochondria *ex vivo* and in whole cells.

* Corresponding author.
E-mail address: eric.goetzman@chp.edu (E.S. Goetzman).

https://doi.org/10.1016/j.redox.2019.101253
Received 8 May 2019; Received in revised form 31 May 2019; Accepted 10 June 2019
Available online 15 June 2019

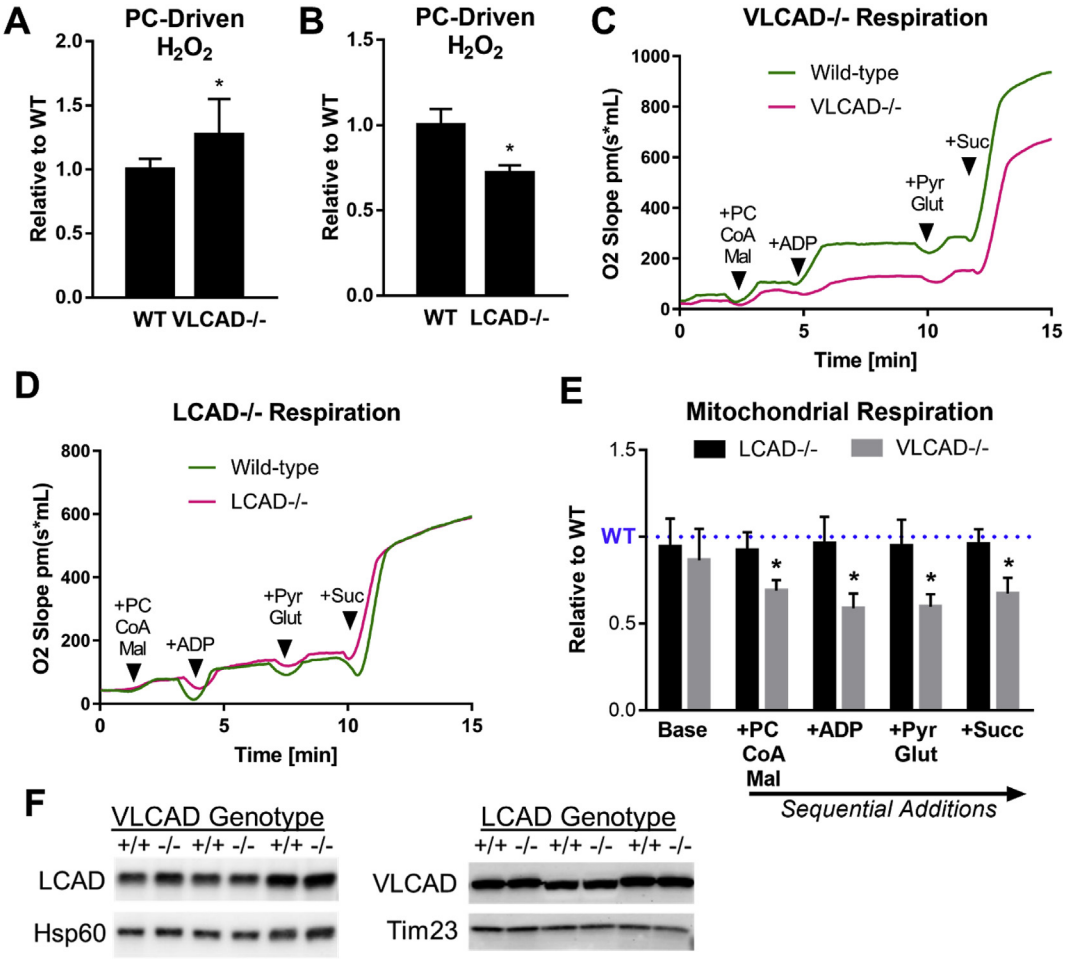

Fig. 1. LCAD is the source of FA-driven H2O2 in mouse liver while VLCAD links FAO to mitochondrial respiration. A, B) Palmitoylcarnitine (PC)-stimulated H_2O_2 release from heavy liver mitochondria isolated from VLCAD−/− and LCAD−/− mice compared to wild-type controls (N = 6), *P < 0.05. H_2O_2 release was normalized to protein concentration and then scaled to wild-type controls. C,D) Representative oxygen consumption trace for VLCAD−/− and LCAD−/− heavy mitochondria using Oroboros high-resolution respirometry; arrows indicate time of addition of the indicated substrates. Mal = malate, Pyr = pyruvate, Glut = glutamate, Succ = succinate. E) Summary data for N = 6 respirometry runs of LCAD−/− and VLCAD−/− heavy mitochondria versus their respective controls. Data were normalized to protein concentration and then scaled to wild-type controls, which were set = 1.0. *P < 0.01. F) Anti-LCAD immunoblot in VLCAD−/− versus wildtype control mouse liver homogenates (left); anti-VLCAD immunoblot in LCAD−/− versus wildtype control mouse liver homogenates (right). Hsp60 is used as a matrix loading control and Tim23 as a membrane loading control for LCAD and VLCAD, respectively. All bar graphs represent means and standard deviations.

2. Results

LCAD is a source of FAO-driven H_2O_2 in mouse liver mitochondria. To determine the relative roles of LCAD and VLCAD in producing mitochondrial H_2O_2, LCAD−/− and VLCAD−/− heavy liver mitochondria were isolated. H_2O_2 production was measured in intact mitochondria in respiratory State 4 using 20 μM palmitoylcarnitine supplemented with 20 μM free coenzyme-A (CoA) to ensure that CoA would not become rate-limiting. Under these conditions, VLCAD−/− heavy mitochondria exhibited significantly increased H_2O_2 production and LCAD−/− mitochondria exhibited significantly decreased H_2O_2 production compared to their respective wild-type mitochondria (Fig. 1A and B). Oroboros high-resolution respirometry was used to measure respiration in the same mitochondrial isolates. VLCAD−/− mitochondria showed significantly impaired State 4 and State 3 respiration on palmitoylcarnitine as well as impaired State 4 respiration with pyruvate, glutamate, and succinate (Fig. 1C,E). Thus, the increase in H_2O_2 seen in VLCAD−/− liver mitochondria are likely due to respiratory chain dysfunction, a phenomenon reported in fibroblasts cultured from patients with VLCAD deficiency [19]. LCAD−/− mitochondria, on the other hand, showed no change in respiratory chain function (Fig. 1D and E). Finally, we confirmed that knocking out VLCAD did not alter expression of LCAD, or vice versa (Fig. 1F).

***LCAD generates H_2O_2* in vitro.** *E coli* expression systems were used to generate His-tagged mouse LCAD (mLCAD), human LCAD (hLCAD), mouse VLCAD (mVLCAD), and human VLCAD (hVLCAD). Among the four enzymes, hLCAD exhibited the lowest palmitoyl-CoA dehydrogenase activity (Fig. 2A) but the highest rate of H_2O_2 formation (Fig. 2B). mLCAD, which is 88% identical in amino acid sequence, produced only half as much H_2O_2 as hLCAD but was twice as active as a dehydrogenase. Enzyme kinetics were used to evaluate the palmitoyl-CoA oxidase capacity of hLCAD as compared to hVLCAD and recombinant human ACOX1, a *bona fide* peroxisomal palmitoyl-CoA oxidase. The oxidase activity of hLCAD followed sigmoidal allosteric kinetics, with a Hill coefficient of 2.2 which indicates cooperativity across hLCAD subunits (Fig. S1A). The hVLCAD data could not be fit with the allosteric model, but rather adhered more closely to the Michaelis-Menten model (Fig. S1B). ACOX1 exhibited allosteric kinetics with a Hill coefficient similar to that of hLCAD (Fig. S1C). The maximum velocity of hLCAD as a palmitoyl-CoA oxidase (V_{max}) was 15-fold higher than that of hVLCAD, yet 54-fold lower than ACOX1. ACOX1 had no detectable activity as a dehydrogenase.

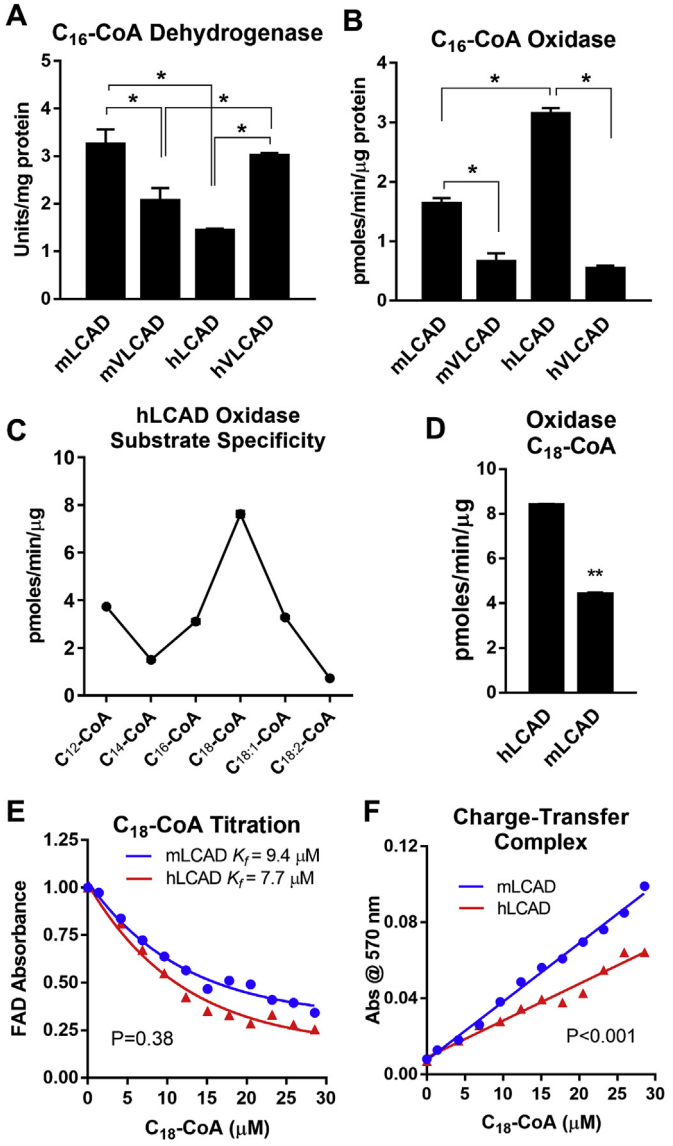

Fig. 2. Human LCAD generates more H2O2 than VLCAD or mouse LCAD. Purified recombinant mouse (m) and human (h) LCAD and VLCAD were compared for enzymatic activity as A) palmitoyl-CoA dehydrogenases and B) palmitoyl-CoA oxidases, respectively, with 25 µM substrate; *P < 0.001. Bars represent means and standard deviations of quadruplicate assays. C) Recombinant hLCAD was assayed as oxidase in quadruplicate across a panel of acyl-CoA substrates. D) Compared to recombinant mLCAD, recombinant hLCAD generates significantly more H_2O_2 when incubated with stearoyl-CoA ($C_{18:0}$); bars represent means and standard deviations of quadruplicate assays, **P < 0.001. E,F) Anaerobic titration of 1 mg/ml recombinant mLCAD and hLCAD proteins with stearoyl-CoA similarly reduces the FAD absorbance peak (E), but hLCAD forms a weaker charge-transfer complex with the enoyl-CoA product than mLCAD (F).

Table 1
Kinetic parameters of hLCAD oxidase/dehydrogenase activities.

hLCAD Activity	Substrate	K_{half} or K_m (µm Palmitoyl-CoA)	V_{max} (nM Per min)	Turnover (min^{-1})
Oxidase	Palmitoyl-CoA	2.1	35.1	0.2
Dehydrogenase	Palmitoyl-CoA	6.8	560	45.2
Oxidase	Stearoyl-CoA	2.1	94.1	0.5
Dehydrogenase	Stearoyl-CoA	19.7	932	55.8

The proclivity of hLCAD for H_2O_2 production was further studied over a range of saturated and unsaturated (oleoyl-CoA, linoleoyl-CoA) acyl-CoA species (Fig. 2C). There was a clear peak in activity with stearoyl-CoA ($C_{18:0}$). Kinetically, H_2O_2 production was twice as fast with stearoyl-CoA compared to palmitoyl-CoA but with the same K_{half} of 2.1 µM (Table 1). As a dehydrogenase, the activity of hLCAD with palmitoyl-CoA and stearoyl-CoA followed Michaelis-Menten kinetics. Interestingly, the V_{max} of hLCAD as a dehydrogenase with stearoyl-CoA was nearly twice that of palmitoyl-CoA, but the K_m was also much higher (19.7 versus 6.8 µM). Turnover rates were calculated from both the oxidase and dehydrogenase kinetic data; comparing these values indicated that hLCAD leaks electrons to oxygen at a rate that is approximately 0.5–1% that of its turnover rate as a dehydrogenase (Table 1).

Electron leakage to oxygen by hLCAD may be due to impaired charge-transfer complex formation. The high rate of H_2O_2 formation by hLCAD with stearoyl-CoA, coupled with its unusual dehydrogenase kinetics with this substrate (i.e., high V_{max} but high K_m), led us to examine the oxidative half-reaction of hLCAD with stearoyl-CoA. In the oxidative half-reaction ACAD enzymes convert acyl-CoA substrate to enoyl-CoA product and the FAD becomes reduced, but the product stays bound in the active site to aid in preventing electron leakage to oxygen. The oxidative half-reaction was measured by titrating the recombinant hLCAD and mLCAD enzymes under anaerobic conditions with increasing amounts of stearoyl-CoA (Fig. 2D). As the LCAD-bound FAD takes on electrons, its absorbance peak at 443 nm quenches while a broad new peak representing the charge-transfer complex forms at ~570 nm [20]. The strength of the charge-transfer complex is determined by the enoyl-CoA product aligning in parallel with the FAD rings [20–22]. The two LCAD proteins showed similar rates of FAD quenching but hLCAD demonstrated a significantly weaker charge-transfer complex (Fig. 2E and F). This may be due to a non-optimal alignment of the FAD rings with the enoyl-CoA product in the hLCAD active site, which under aerobic conditions could allow greater access of oxygenated solvent to the FAD and thus greater H_2O_2 formation.

LCAD is expressed in human liver. LCAD is widely expressed in rodents, while human LCAD expression is more restricted. Human type II pneumocytes of the lung express LCAD [23], while key FAO-reliant tissues such as heart and muscle do not [14,15]. LCAD mRNA has been observed in several human tissues including breast, kidney, liver, lung, pancreas, prostate, and thyroid, but expression at the protein level has not been confirmed [24,25]. To determine which human tissues may experience LCAD-driven H_2O_2 *in vivo,* we obtained a panel of commercially prepared human tissue lysates representing mRNA-positive tissues and probed it for LCAD antigen by immunoblot. Among the tissues tested, hLCAD protein levels were clearly the highest in liver followed by kidney, lung, pancreas, and prostate, while thyroid and breast were negative for hLCAD (Fig. 3A). LCAD expression in human liver was confirmed by immunoblotting primary human and mouse hepatocytes (Fig. 3B). The anti-rat LCAD antibody used for this experiment demonstrated similar reactivity to both mouse and human recombinant LCAD proteins (Fig. 3C); subsequent densitometric analysis of the immunoblot in Fig. 3B indicated that LCAD abundance in human hepatocytes is about one-third that of mouse hepatocytes (Fig. 3D). The inter-species difference in LCAD antigen was corroborated by enzyme activity assays in liver homogenates using the LCAD-specific substrate 2,6-dimethylheptanoyl-CoA [26], which revealed 2.5-fold less activity in human liver compared to mouse (Fig. 3E). Together these data indicate a larger role for LCAD in human liver than previously thought [14,15]. hLCAD may therefore contribute to mitochondrial H_2O_2 production in human liver.

hLCAD increases H_2O_2 in a human liver cell line. Commonly used human liver cell lines such as HepG2 are derived from hepatocellular carcinomas (HCCs) which have been reported to downregulate LCAD mRNA [16,17]. To mechanistically interrogate the ability of hLCAD to generate H_2O_2 in human cells, the expression of hLCAD was restored in

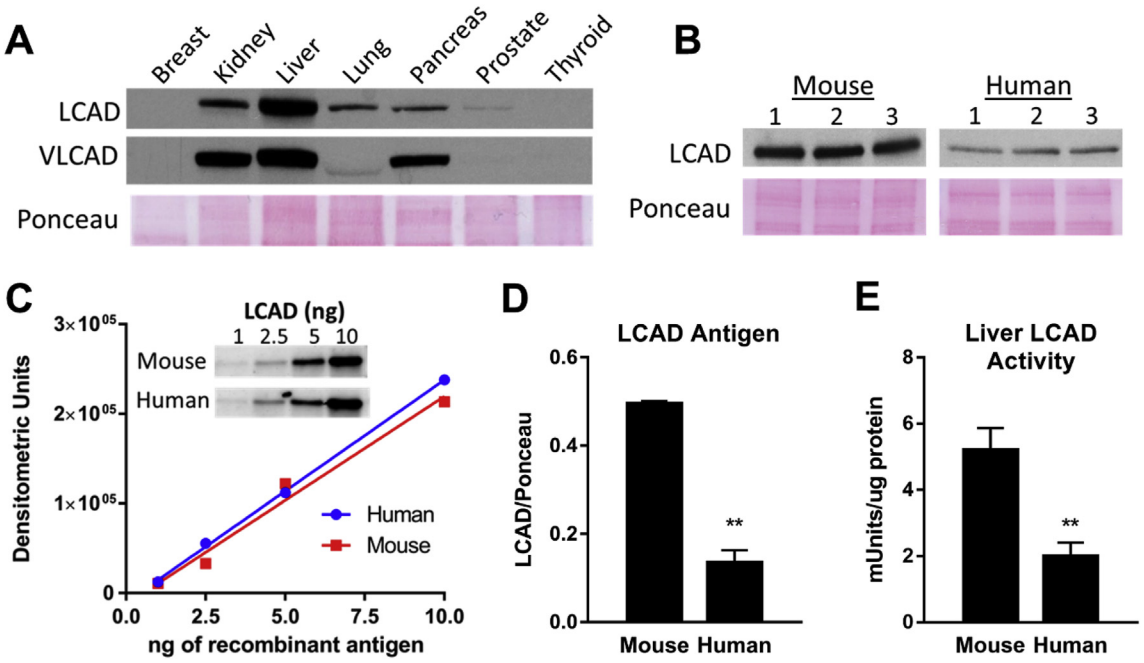

Fig. 3. LCAD is highly expressed in human liver. A) 25 μg of protein from commercially sourced human tissue lysates were immunoblotted for LCAD and VLCAD. B) 25 μg of primary hepatocyte lysates from three humans and three mice were immunoblotted for LCAD and VLCAD (note that the samples were run on the same gel, but the image was cropped for clarity of presentation). C) A concentration series (1–10 ng) of recombinant mLCAD and hLCAD were blotted with anti-rat LCAD antibody to demonstrate that the antibody equally recognizes both species of LCAD protein. D) densitometry was used to compare the intensity of the LCAD bands in panel B to compare LCAD protein expression across species. **P < 0.001. E) hLCAD enzymatic activity detected in human versus mouse liver lysates using the LCAD-specific substrate 2,6-dimethylheptanoyl-CoA. N = 3 liver lysates were assayed in duplicate, **P < 0.001. All bar graphs represent means and standard deviations.

the HepG2 cell line using an hLCAD-Flag expression vector. Palmitoyl-CoA dehydrogenase activity in HepG2 lysates, representing the combined activities of hLCAD and hVLCAD, was significantly increased after hLCAD-Flag transfection (Fig. 4A), and correspondingly, so was total FAO flux measured with ^{3}H-palmitate (Fig. 4B). Enzyme activity with octanoyl-CoA, the preferred substrate of medium-chain acyl-CoA dehydrogenase (MCAD), was measured as a negative control and was not different between empty vector and hLCAD-Flag transfected cells (Fig. 4A). hLCAD-Flag transfected HepG2 cells displayed significantly higher basal production of H_2O_2 and this difference was exacerbated by a 1-h incubation with 20 μM palmitoylcarnitine plus CoA (Fig. 4C). Similarly, incubation with 20 μM palmitate-BSA significantly increased H_2O_2 in hLCAD-Flag transfected cells, indicating that free fatty acids can also induce H_2O_2 through hLCAD (Fig. S2A).

While LCAD-Flag transfection was sufficient to increase FAO-driven H_2O_2 in HepG2 cells, it is possible that the downstream enzymes may be contributing to the observed H_2O_2. Re-expression of hLCAD in HepG2 cells did not alter expression of VLCAD, ETF, or ETFDH (Fig. 4D); however, increased electron flux through ETF/ETFDH may have contributed to H_2O_2 production, which could not be experimentally distinguished from LCAD-generated H_2O_2 in the HepG2 model. *In vitro,* we observed that a mixture of purified recombinant human ETF, recombinant hLCAD, and palmitoyl-CoA produced significantly more H_2O_2 than a mixture of hLCAD and palmitoyl-CoA without ETF (Fig. 4E). Thus, LCAD and ETF may synergize to produce H_2O_2 in the HepG2 model. Regarding the electron transport chain, HepG2 cells transfected with LCAD-Flag had the same basal oxygen consumption rate (OCR) as control HepG2 cells (Fig. S2B). There was a non-significant trend toward higher "spare reserve capacity" in LCAD-Flag expressing cells, defined as the OCR after addition of the uncoupler FCCP. The contribution of Complex III to H_2O_2 formation, which receives the electrons from the LCAD-ETF-ETFDH axis, was determined using the inhibitor S3QEL2. S3QEL2 eliminates superoxide from Complex III without blocking oxidative phosphorylation [27]. S3QEL2 inhibited H_2O_2 release by 65–70% in both control and LCAD-Flag transfected HepG2 cells incubated with palmitoylcarnitine + CoA, but H_2O_2 production still remained significantly higher in hLCAD-Flag expressing cells (Fig. 4F).

3. Discussion

Several recent investigations have confirmed the existence of an electron transport chain-independent, matrix-localized source of FAO-driven mitochondrial H_2O_2 [3,5–7]. This matrix source is ascribed to ETFDH, ETF, and/or the ACAD enzymes that use ETF as a common electron acceptor. *In vitro,* ETF and VLCAD have been shown to leak electrons to oxygen [13,28]. Here, we add LCAD to the list of H_2O_2-generating ACAD enzymes and show that it generates ~15-fold more H_2O_2 than VLCAD. Our loss-of-function (LCAD −/− liver mitochondria) and gain-of-function (LCAD-Flag transfected HepG2 cells) experiments indicate that the presence/absence of LCAD can significantly alter the rate of H_2O_2 generation in complex systems. However, we could not definitively discern between direct LCAD-generated H_2O_2 and H_2O_2 produced downstream by ETF, ETFDH, and the respiratory chain. Evidence supporting electron leakage from ETF is currently limited to data generated with purified ETF protein. For ETFDH, the evidence is strictly circumstantial, based on data indicating that there is superoxide/H_2O_2 formation somewhere upstream of Complex III, which could be either the ACADs, ETF, ETFDH, or all of these working in concert [3,5–7]. Arguing against as significant role for ETFDH is the observation that, while mutant forms of ETFDH produce oxidative stress when overexpressed in cultured cells, the wildtype enzyme does not [29]. Future loss-of-function and gain-of-function studies for the ACADs, ETF, and ETFDH, alone and in combination, are needed in order to elucidate the relative roles of these enzymes in producing reactive oxygen species *in vivo*.

Further complicating matters is the fact that the specific sites of FAO-driven mitochondrial H_2O_2 formation appear to differ widely across tissue types, particularly with regards to the electron transport chain [6,30,31]. Here, we focused exclusively on liver, using either

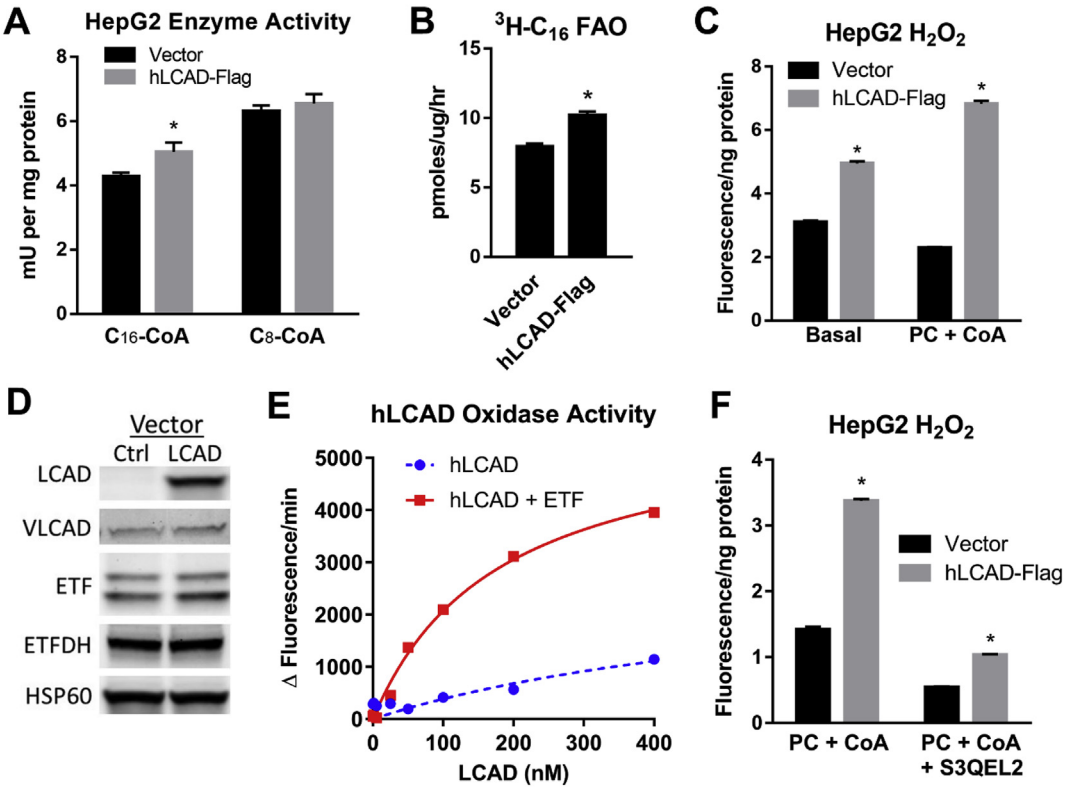

Fig. 4. LCAD increases H_2O_2 in a human liver cell line. A) HepG2 cells were transiently transfected with either empty vector or hLCAD-Flag and tested in quadruplicate for palmitoyl-CoA (C_{16}-CoA) and octanoyl-CoA (C_8-CoA) dehydrogenase activities. hLCAD-Flag transfection increased long-chain but not medium chain activity. B) hLCAD-Flag expressing cells have higher flux through the mitochondrial long-chain FAO pathway measured with ^{3}H-palmitate-BSA. Data shown represent five wells of transfected cells. C) hLCAD-Flag expressing cells displayed significantly higher H_2O_2 release to the media at baseline and after stimulation for 1 h with 20 μM palmitoylcarnitine (PC) plus free coenzyme-A. D) Immunoblotting of HepG2 cellular lysates confirmed the re-expression of hLCAD after hLCAD-Flag transfection. hLCAD-Flag transfection did not alter expression of other flavoproteins in the long-chain FAO pathway. Shown are representative blots. Blots were repeated either three times (VLCAD, ETF) or twice (ETFDH) with different protein loading amounts. Densitometry was used to calculate mean expression values in LCAD-Flag cells relative to vector-only control, which were 0.99, 1.00, and 0.99 for VLCAD, ETF, and ETFDH, respectively. Heat-shock protein-60 (HSP60) served as loading control. E) H_2O_2 generation by a concentration series (0–400 nM) of recombinant hLCAD incubated with 25 μM palmitoyl-CoA ± 1.5 μM recombinant human ETF. F) Vector-only control and hLCAD-Flag transfected HepG2 cells were incubated with 20 μM PC + CoA for 1 hr ± the Complex III inhibitor S3QEL2, and H_2O_2 assayed with Amplex red. The experiment measured 4 wells of cells per condition. All bars in this figure represent means and standard deviations; *$P < 0.01$. All cell culture experiments were repeated 2–3 times with similar results. (For interpretation of the references to colour in this figure legend, the reader is referred to the Web version of this article.)

isolated mouse liver mitochondria or the liver-derived human cancer cell line HepG2. Tahara et al. [30] demonstrated no effect of respiratory chain inhibitors on palmitoylcarnitine-induced H_2O_2 release from rat liver mitochondria. In contrast, the study of Schonfeld et al. [31] implicated Complex III as source of palmitoylcarnitine-induced H_2O_2 in liver mitochondria based on a significant increase in the presence of antimycin-A. The primary difference between these two studies was the inclusion of malate with palmitoylcarnitine in the Schonfeld study, which would drive FAO-generated acetyl-CoA into the TCA cycle and thus produce a more reduced state of the electron transport chain. In the present study, our mouse liver mitochondria experiment more closely followed the conditions of Tahara et al. [30], with no addition of malate. In the whole-cell studies, we chose to use S3QEL2 as a Complex III inhibitor, as this inhibitor can inhibit superoxide production without blocking oxidative phosphorylation [27]. S3QEL2 reduced palmitoylcarnitine-induced H_2O_2 formation by about two-thirds regardless of LCAD-Flag expression. However, the presence of LCAD-Flag still doubled H_2O_2 release even with Complex III inhibited. Based on this, we propose that LCAD-Flag is directly contributing to the H_2O_2 rather than merely driving more reducing equivalents into the respiratory chain. This effect may involve amplification of H_2O_2 generation by ETF.

In summary, we have shown that LCAD, whose physiological role in humans remains controversial [14,15], produces H_2O_2 in response to long-chain fatty acids. We further show that LCAD is co-expressed with VLCAD in human liver. There is evidence that VLCAD binds to cardiolipin on the inner mitochondrial membrane and interacts with the electron transport chain in a higher-order FAO complex [32]. LCAD, being outside of this complex, may occupy a unique niche as a generator of mitochondrial metabolic H_2O_2 for signaling purposes. This signaling role could explain why expression of LCAD, but not other ACAD family members or other mitochondrial FAO enzymes, is specifically lost in several cancers including HCC [16,17]. In one recent study, re-expressing hLCAD in HCC was shown to increase oxidative stress and slow proliferation [17]. Future work will focus on delineating the signaling role of hLCAD *in vivo* and further explore the utility of LCAD re-expression as a therapeutic target for driving metabolic H_2O_2 signaling.

4. Materials & Methods

Animals—The mouse strains used have been previously described [23,33]. All breeding and experimental protocols were approved by the University of Pittsburgh Institutional Animal Care and Use Committee. Animals used were males age 6–10 weeks.

Isolation of mitochondria—Fresh tissue was mince and homogenized in 0.2 M mannitol, 50 mM sucrose, 10 mM KCl, 1 mM EDTA, 2.5 mM fatty acid-free BSA, 10 mM Hepes, pH 7.4. Unbroken cells were cleared by centrifugation at 1000 × *g*, then the heavy mitochondrial fraction

was pelleted by centrifugation at 3000 × *g*. The resulting pellet was dispersed in MiR05 mitochondrial respiration buffer [34] and immediately used.

Oroboros respirometry— Mitochondrial respiration was measured in an Oroboros Oxygraph-2K [34]. Substrate additions were palmitoylcarnitine (25 μM), coenzyme-A (25 μM), and malate (2 mM) all together, followed by 5 mM ADP to stimulate state 3 respiration. Next, 5 mM pyruvate and 10 mM glutamate (10 mM) were added to drive Complex I and 10 mM succinate to assess the combined activity of Complex I + II. Oxygen consumption rates were first normalized to protein content, and then rates for the knockout mitochondria scaled to wild-type.

Recombinant protein expression—The four recombinant ACADs and human ETF were expressed in *E coli* and purified as described [33,35,36]. The vector for human ACOX1 was a kind gift of Dr. Mustapha Cherkaoui-Malki (University of Burgundy, Dijon, France) [37].

H_2O_2 generation—For recombinant proteins, 1 μg of protein was added to 50 mM phosphate buffer pH 7.0 containing HRP (1 U/ml) and Amplex UltraRed (50 μM) at 30 °C. Reactions were started by addition of acyl-CoA substrate and fluorescence was monitored for 30 min. For mitochondria, 100 μM phenylmethylsulfonyl fluoride was added to inhibit mitochondrial carboxylesterase [38], 1 μM 10, 12-tricosadiynoic acid (TDYA) to inhibit peroxisomal acyl-CoA oxidase [39], and 5 mM 3-amino-1,2,4-triazole (3-AT) to inhibit catalase [40].

ETF fluorescence reduction assay—The anaerobic electron transfer flavoprotein (ETF) fluorescence reduction assay was used to measure dehydrogenase activities [35] with either 150 ng of purified recombinant protein or 200 μg of total liver protein. All acyl-CoA substrates were from Sigma (St. Louis, MO) except for 2,6-dimethylheptanoyl-CoA (Toronto Research Chemicals, Toronto, ON).

Anaerobic substrate titration— Titrations were done as described in stoppered, degassed quartz cuvettes using a Jasco V-650 spectrophotometer [35]. The protein concentration was 1 mg/ml.

Western blotting—Human breast, kidney, liver, lung, pancreas, prostate, and thyroid lysates were purchased from G-Biosciences (St. Louis, MO). Primary mouse hepatocyte lysates and primary human hepatocyte lysates were gifts of Drs. Edward Prochownik and Henry Dong, respectively (Children's Hospital of Pittsburgh). Rabbit anti-sera raised against native rat LCAD, ETF, and recombinant human VLCAD were gifts of Dr. Jerry Vockley (Children's Hospital of Pittsburgh) and were used at 1:2000 dilution. Anti-actin (Proteintech HRP60008), anti-Tim23 (BD Biosciences 611222), anti-HSP60 (Cell Signaling 12165), and anti-ETFDH (Sigma SAB1303142) were used at the manufacturers' recommended dilutions.

Expression of hLCAD in HepG2 cells. Expression of flag-tagged human LCAD in the vector pcDNA3.1 has been previously described [41]. Empty pcDNA3.1 vector served as control. Transfected cells were used for acyl-CoA dehydrogenase assays as described above and for whole-cell ^{3}H-palmitate oxidation according to our protocol [42]. The Seahorse assay was done in a Seahorse XF96 analyzer, with 15,000 cells plated per well the day before the assay. Cells were exposed to 20 μM palmitoyl-L-carnitine and 20 μM free CoA for 1 h in standard Seahorse basal medium (10 mM Glucose, 1 mM sodium pyruvate, 2 mM L-Glutamine in DMEM without phenol red), and then were immediately assayed in this same medium. Inhibitor injected during Seahorse assay were oligomycin (1 μM), FCCP (1 μM), 2-deoxyglucose (50 mM), and rotenone (0.5 μM). Six wells were analyzed for each vector-transfected and LCAD-Flag transfected cells and normalized to protein content to control for inter-well variations in plating of HepG2 cells, which tend to form clumps during passaging.

For H_2O_2 generation, the transfected cells were treated with 20 μM palmitoyl-L-carnitine and 20 μM free CoA for 1 h in the presence of 3-AT and TDYA to inhibit catalase and ACOX1, respectively. In some experiments 9 μM of the Complex III inhibitor S3QEL2 was also added [27]. At the end of the 1-h incubation the cells were lysed and assayed for H_2O_2 generation as described above for mouse liver mitochondria.

Data analysis and statistics— All curve-fitting of kinetic data and subsequent determination of V_{max}, K_m, K_{half}, and Hill coefficients was done using GraphPad Prism 7.0. Catalytic efficiency was calculated as described [43]. Pairwise comparisons were made by *t*-test using Graphpad Prism 7.0.

Author Contributions

Y.Z. planned and executed experiments and assisted with data analysis and writing of the manuscript. S.S.B. and M.E.B. performed experiments. E.S.G. oversaw the studies, analyzed data, and prepared the manuscript.

Conflict of interest

The authors have no conflicts of interest to report.

Acknowledgements

This work was funded by the National Institutes of Health DK090242 (ESG).

Appendix A. Supplementary data

Supplementary data to this article can be found online at https://doi.org/10.1016/j.redox.2019.101253.

References

[1] Q. Chen, et al., Oxidative stress mediated by lipid metabolism contributes to high glucose-induced senescence in retinal pigment epithelium, Free Radic. Biol. Med. 130 (2018) 48–58.
[2] S. Cortassa, S.J. Sollott, M.A. Aon, Mitochondrial respiration and ROS emission during beta-oxidation in the heart: an experimental-computational study, PLoS Comput. Biol. 13 (6) (2017) e1005588.
[3] I.V. Perevoshchikova, et al., Sites of superoxide and hydrogen peroxide production during fatty acid oxidation in rat skeletal muscle mitochondria, Free Radic. Biol. Med. 61 (2013) 298–309.
[4] P. Schonfeld, L. Wojtczak, Brown adipose tissue mitochondria oxidizing fatty acids generate high levels of reactive oxygen species irrespective of the uncoupling protein-1 activity state, Biochim. Biophys. Acta 1817 (3) (2012) 410–418.
[5] M.G. Rosca, et al., Oxidation of fatty acids is the source of increased mitochondrial reactive oxygen species production in kidney cortical tubules in early diabetes, Diabetes 61 (8) (2012) 2074–2083.
[6] E.L. Seifert, et al., Electron transport chain-dependent and -independent mechanisms of mitochondrial H2O2 emission during long-chain fatty acid oxidation, J. Biol. Chem. 285 (8) (2010) 5748–5758.
[7] A.R. Cardoso, P.A. Kakimoto, A.J. Kowaltowski, Diet-sensitive sources of reactive oxygen species in liver mitochondria: role of very long chain acyl-CoA dehydrogenases, PLoS One 8 (10) (2013) e77088.
[8] M.D. Brand, The sites and topology of mitochondrial superoxide production, Exp. Gerontol. 45 (7–8) (2010) 466–472.
[9] S.M. Houten, R.J. Wanders, A general introduction to the biochemistry of mitochondrial fatty acid beta-oxidation, J. Inherit. Metab. Dis. 33 (5) (2010) 469–477.
[10] M.K. Montgomery, et al., Contrasting metabolic effects of medium- versus long-chain fatty acids in skeletal muscle, J. Lipid Res. 54 (12) (2013) 3322–3333.
[11] J. Liu, et al., Long-chain fatty acid activates hepatocytes through CD36 mediated oxidative stress, Lipids Health Dis. 17 (1) (2018) 153.
[12] B. Wang, et al., Effects of long-chain and medium-chain fatty acids on apoptosis and oxidative stress in human liver cells with steatosis, J. Food Sci. 81 (3) (2016) H794–H800.
[13] P.A. Kakimoto, et al., H2O2 release from the very long chain acyl-CoA dehydrogenase, Redox Biol 4 (2015) 375–380.
[14] M. Chegary, et al., Mitochondrial long chain fatty acid beta-oxidation in man and mouse, Biochim. Biophys. Acta 1791 (8) (2009) 806–815.
[15] A.C. Maher, et al., Low expression of long-chain acyl-CoA dehydrogenase in human skeletal muscle, Mol. Genet. Metab. 100 (2) (2010) 163–167.
[16] C. Allain, et al., Integrative genomic analysis identifies the core transcriptional hallmarks of human hepatocellular carcinoma, Cancer Res. 76 (21) (2016) 6374–6381.
[17] Huang, et al., HIF-1-mediated suppression of acyl-CoA dehydrogenases and fatty acid oxidation is critical for cancer progression, Cell Rep. 8 (6) (2014) 1930–1942.
[18] V.K. Hill, et al., Genome-wide DNA methylation profiling of CpG islands in breast cancer identifies novel genes associated with tumorigenicity, Cancer Res. 71 (8) (2011) 2988–2999.
[19] B. Seminotti, et al., Mitochondrial energetics is impaired in very long-chain acyl-CoA dehydrogenase deficiency and can be rescued by treatment with mitochondria-

targeted electron scavengers, Hum. Mol. Genet. 28 (6) (15 March 2019) 928–941, https://doi.org/10.1093/hmg/ddy403.
[20] S. Ghisla, C. Thorpe, Acyl-CoA dehydrogenases. A mechanistic overview, Eur. J. Biochem. 271 (3) (2004) 494–508.
[21] S.M. Lau, R.K. Brantley, C. Thorpe, The reductive half-reaction in Acyl-CoA dehydrogenase from pig kidney: studies with thiaoctanoyl-CoA and oxaoctanoyl-CoA analogues, Biochemistry 27 (14) (1988) 5089–5095.
[22] S.M. Lau, C. Thorpe, The nature of enzyme-substrate complexes in acyl-coenzyme A dehydrogenases, Arch. Biochem. Biophys. 262 (1) (1988) 293–297.
[23] E.S. Goetzman, et al., Long-chain acyl-CoA dehydrogenase deficiency as a cause of pulmonary surfactant dysfunction, J. Biol. Chem. 289 (15) (2014) 10668–10679.
[24] M. He, et al., A new genetic disorder in mitochondrial fatty acid beta-oxidation: ACAD9 deficiency, Am. J. Hum. Genet. 81 (1) (2007) 87–103.
[25] Z. Li, et al., Integrated analysis of gene expression and methylation profiles of 48 candidate genes in breast cancer patients, Breast Canc. Res. Treat. 160 (2) (2016) 371–383.
[26] R.J. Wanders, et al., 2,6-Dimethylheptanoyl-CoA is a specific substrate for long-chain acyl-CoA dehydrogenase (LCAD): evidence for a major role of LCAD in branched-chain fatty acid oxidation, Biochim. Biophys. Acta 1393 (1) (1998) 35–40.
[27] A.L. Orr, et al., Suppressors of superoxide production from mitochondrial complex III, Nat. Chem. Biol. 11 (11) (2015) 834–836.
[28] J.V. Rodrigues, C.M. Gomes, Mechanism of superoxide and hydrogen peroxide generation by human electron-transfer flavoprotein and pathological variants, Free Radic. Biol. Med. 53 (1) (2012) 12–19.
[29] N. Cornelius, et al., Molecular mechanisms of riboflavin responsiveness in patients with ETF-QO variations and multiple acyl-CoA dehydrogenation deficiency, Hum. Mol. Genet. 21 (15) (2012) 3435–3448.
[30] E.B. Tahara, F.D. Navarete, A.J. Kowaltowski, Tissue-, substrate-, and site-specific characteristics of mitochondrial reactive oxygen species generation, Free Radic. Biol. Med. 46 (9) (2009) 1283–1297.
[31] P. Schonfeld, et al., Mitochondrial fatty acid oxidation and oxidative stress: lack of reverse electron transfer-associated production of reactive oxygen species, Biochim. Biophys. Acta 1797 (6–7) (2010) 929–938.
[32] Y. Wang, et al., Evidence for physical association of mitochondrial fatty acid oxidation and oxidative phosphorylation complexes, J. Biol. Chem. 285 (39) (2010) 29834–29841.
[33] Y. Zhang, et al., SIRT3 and SIRT5 regulate the enzyme activity and cardiolipin binding of very long-chain acyl-CoA dehydrogenase, PLoS One 10 (3) (2015) e0122297.
[34] Y. Zhang, et al., Lysine desuccinylase SIRT5 binds to cardiolipin and regulates the electron transport chain, J. Biol. Chem. 292 (24) (2017) 10239–10249.
[35] S.S. Bharathi, et al., Sirtuin 3 (SIRT3) protein regulates long-chain acyl-CoA dehydrogenase by deacetylating conserved lysines near the active site, J. Biol. Chem. 288 (47) (2013) 33837–33847.
[36] H.M. Hoard-Fruchey, et al., Mammalian electron transferring flavoprotein.-flavoprotein dehydrogenase complexes observed by microelectrospray ionization-mass spectrometry and surface plasmon resonance, J. Biol. Chem. 279 (14) (2004) 13786–13791.
[37] D. Oaxaca-Castillo, et al., Biochemical characterization of two functional human liver acyl-CoA oxidase isoforms 1a and 1b encoded by a single gene, Biochem. Biophys. Res. Commun. 360 (2) (2007) 314–319.
[38] S. Miwa, et al., Carboxylesterase converts Amplex red to resorufin: implications for mitochondrial H2O2 release assays, Free Radic. Biol. Med. 90 (2016) 173–183.
[39] J. Zeng, et al., Specific inhibition of acyl-CoA oxidase-1 by an acetylenic acid improves hepatic lipid and reactive oxygen species (ROS) metabolism in rats fed a high fat diet, J. Biol. Chem. 292 (9) (2017) 3800–3809.
[40] E. Margoliash, A. Schejter, Kinetics of irreversible inhibition of catalase, Biochem. J. 74 (1960) 349–350.
[41] M.D. Hirschey, et al., SIRT3 regulates mitochondrial fatty-acid oxidation by reversible enzyme deacetylation, Nature 464 (7285) (2010) 121–125.
[42] M.B. de Moura, et al., Overexpression of mitochondrial sirtuins alters glycolysis and mitochondrial function in HEK293 cells, PLoS One 9 (8) (2014) e106028.
[43] E.S. Goetzman, et al., Convergent evolution of a 2-methylbutyryl-CoA dehydrogenase from isovaleryl-CoA dehydrogenase in Solanum tuberosum, J. Biol. Chem. 280 (6) (2005) 4873–4879.